Energy and lifetime of one-electron multicharged-ion states in front of an Al surface

A. G. Borisov,[1] R. Zimny,[2] D. Teillet-Billy,[3] and J. P. Gauyacq[3]
[1]*Institut für Physik, Humboldt Universität zu Berlin, Invalidenstrasse 110, D-10115, Berlin, Germany*
[2]*Institut für Kernphysik, Universität Münster, Wilhelm-Klem-Strasse 9, D-48149 Münster, Germany*
[3]*Laboratoire des Collisions Atomiques et Moléculaires (Unité de Recherches associée au CNRS No. 281), Université de Paris-Sud, Bâtiment 351, 91405 Orsay Cedex, France*
(Received 25 July 1995)

The energy and width of one-electron multicharged-ion states interacting with an Al surface are determined using the nonperturbative coupled angular mode method. The case of the He^+, Li^{2+}, and O^{7+} states is studied. The various states within the n manifolds mix to form hybrids with very different energies and widths. The hybridization within the manifolds can be analyzed in terms of Stark mixing.

PACS number(s): 34.50.Dy, 34.70.+e

I. INTRODUCTION

The interaction of multicharged ions with solid surfaces has been the subject of extensive experimental and theoretical studies. Detailed experimental data are available on the electron and ion emission in multicharged-ion impact on conducting [1–6] or dielectric [7–9] surfaces. The effect of the image charge interaction between multicharged ions and metal [3,10–12] or dielectric [13] surfaces has also been studied and discussed. The capture of the target electrons by the ingoing ion plays a crucial role in all these phenomena. Because of the large number of electrons involved in the multicharged ion-surface interaction, a theoretical description is rather complicated. Presently, a rather appealing and efficient model is the semiclassical ''over the barrier'' model [14,15]. It assumes that electron capture by the ion only occurs when it is classically allowed. Though very simple, this model is found to reproduce noticeably well the experimental observations, e.g., hollow atom formation and Auger electron emission [3,4,14], as well as image charge acceleration of multicharged ions towards the surface [10–12].

Some attempts have been made to describe the charge transfer (CT) process between a multicharged ion and a metal surface in a way similar to that used to describe the CT process for a singly charged ion; this consists in calculating the energy and the widths of the various states of the ion interacting with the surface. The widths of the states correspond to the various charge transfer rates and these can be used in a semiclassical rate equation [16–18] that describes the time evolution of the population of the various charge states during the ion-surface collision. The first calculations of multicharged ion states interacting with a metal surface were performed within a certain number of approximations allowing for asymptotic and semiclassical approaches [19,20]. More recently, an extensive study of the level widths within the large-n manifolds (n is the principal quantum number) was performed using the perturbative method, originally proposed by Gadzuk [21]. It allowed for a discussion of scaling laws and universal behavior for the level widths [22–24]. All the calculations mentioned above concern one-electron states, i.e., they apply to the capture of an electron by bare ions.

Recently two nonperturbative methods were developed that can determine the properties of atomic (or ionic) states in front of the metal surface. These are the complex scaling method of Nordlander and Tully [25,26] and the coupled angular mode (CAM) method of Teillet-Billy and Gauyacq [27]. These two methods have been found to yield the same predictions when applied to the same system. In particular, the $n=2$ and 3 manifolds of hydrogen interacting with an Al surface was studied by both methods [25,28]. Within each manifold, the states with the same symmetry were found to mix together to form hybrids with extremely different lifetimes. This could be interpreted using perturbation theory for degenerate states [28] as the effect of a Stark mixing within the manifold, at least for the smallest atom-surface distances. The results obtained with the nonperturbative methods were found to be quite different from those obtained with perturbative methods.

In the present paper, we report on a theoretical study using the CAM method of various manifolds of one-electron multicharged of one-electron multicharged-ion states interacting with an Al surface. Results are presented for the $He^+(n=2$ and $n=4)$, $Li^{2+}(n=5)$, and $O^{7+}(n=9)$ manifolds. These manifolds were chosen as representative of cases with different charges and comparable energies. The energies of the states in these manifolds are in the range between a few eV and 10 eV and thus, taking into account the image-charge displacement of the energy (see below), these states are the active ones in the CT process on an Al surface. Inside the manifolds, the results are analyzed in terms of linear Stark mixing. The levels considered in the present work are one-electron states; they are the ones involved in the one-electron capture process by a bare ion approaching an Al surface. The properties of the one-electron states studied here can then be used to study the first step of the neutralization of a multicharged ion approaching an Al surface and, for example, to study the distance of the first electron capture. However, in the case of a multicharged ion, one expects the complete neutralization process to involve many electrons and multielectron processes to play a role. A detailed quantitative study of these processes is out of the scope of the present work.

II. CALCULATION OF THE ENERGY AND WIDTH OF IONIC STATES IN FRONT OF THE METAL SURFACE

A. General

Details on the CAM method can be found in earlier publications [27,28]. Here we will only briefly outline the method and its particular application to the case of a multicharged ion interacting with a metal surface. Basically, the CAM method is a scattering method, which consists in studying the electron scattering in the compound potential, created by the metal surface and the ionic core. The states of the ion appear as resonances in this scattering and their energies and widths are associated with the energies and widths of the resonances. Atomic units are used below, unless otherwise stated.

B. Potentials

To construct the potential V acting on the electron we use three terms (see also [28]):

$$V = V_{e\text{-}i} + V_{e\text{-}s} + \Delta V_{e\text{-}s}, \tag{1}$$

where $V_{e\text{-}i}$ is the electron interaction with the ion core; $V_{e\text{-}s}$ is the electron interaction with the surface; ΔV_{e-s} is the modification of the electron-surface interaction due to the presence of the ion. For all the systems studied here, V_{e-i} is a pure Coulomb potential, given by

$$V_{e\text{-}i} = -Q/r, \tag{2}$$

where Q is the charge of the ion core and r is the electron distance from the ion.

To describe the electron-surface interaction we use the local potential given by Jennings, Jones, and Weinert [29]. It is only a function of z, the electron-surface distance. The analytical expression given in [29] contains three parameters that we took from [29] corresponding to the Al surface: the bottom of the metal conduction band is $U = 15.9$ eV, the size of the surface region is given by $\lambda = 1.0$ a.u., and the third parameter, giving the position of the image reference plane, has been incorporated in the definition of the ion-surface distance, this distance R is measured from the image reference plane.

The third term $\Delta V_{e\text{-}s}$ is taken to be the interaction of the electron with the classical image of the core:

$$\Delta V_{e\text{-}s} = Q/D, \tag{3}$$

where D is the electron distance from the image of the ion.

The above expressions correspond to the case where the electron is outside the metal. On the surface, the two potentials $V_{e\text{-}i}$ and $\Delta V_{e\text{-}s}$ cancel each other (the surface plane is chosen as the image reference plane) and they vanish inside the metal. The expression (3) corresponds to the case of a perfect metal. In fact, the charges induced in the metal by the presence of the ion core are spread over the surface region. An approach similar to that used in [25,26] could be used. However, for the present study of rather high-lying states, the use of the approximate expression (3) does not introduce a large error (see [28]); indeed, only the large-distance part of the potentials is important in determining the ion properties [30].

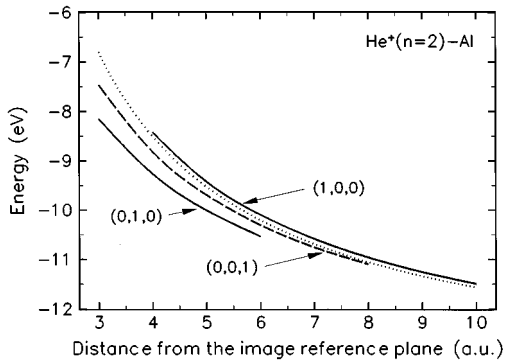

FIG. 1. Energies of the He^+ $(n=2)$ states in front of an Al surface. Solid lines: $m=0$ states; dashed line: $|m|=1$ state; dotted line: energy, obtained from the image shift, given by the first term in (7). Parabolic notations for the states are also given.

C. Scattering calculation

The wave function of the scattered electron is expanded over the spherical harmonics $Y_{l,m}(\theta,\varphi)$, centered around the ion:

$$\Psi = \sum_l \frac{1}{r} F_l(r) Y_{l,m}(\theta,\varphi). \tag{4}$$

We use for the quantization axis an axis normal to the surface and going through the center of the ion. In this case the system is of cylindrical symmetry and m, the projection of the angular momenta l on the quantization axis, is a good quantum number. Thus, the expansion (4) is restricted to the l quantum number; m is fixed and corresponds to the symmetry of the state that is studied. Substitution of the expansion (4) in the Schrödinger equation results in the following set of coupled equations for the radial parts:

$$-\frac{1}{2}\frac{d^2}{dr^2}F_l(r) + \sum_{l'} \langle l,m|V|l',m\rangle F_{l'}(r) = \left(E - \frac{l(l+1)}{2r^2}\right) F_l(r), \tag{5}$$

where E is the energy of the colliding electron.

At small r distances, the $F_l(r)$ is a regular Coulomb wave at the energy $E - \langle l,m|V_{e\text{-}s} + \Delta V_{e\text{-}s}|l,m\rangle$ (the matrix element is evaluated at the point $r=0$). From the solution of Eq. (5) one gets the scattering matrix S; its energy dependence displays resonances, the analysis of which yields the energy and width of the ionic states.

III. RESULTS AND DISCUSSION

A. He^+ $n=2$ and $n=4$ manifolds

Figures 1 and 2 present the energies and the widths of the states in the He^+ $n=2$ manifolds in front of an Al surface. For each state, due to the use of the CAM method, the calculation could not be performed for values of R, the atom

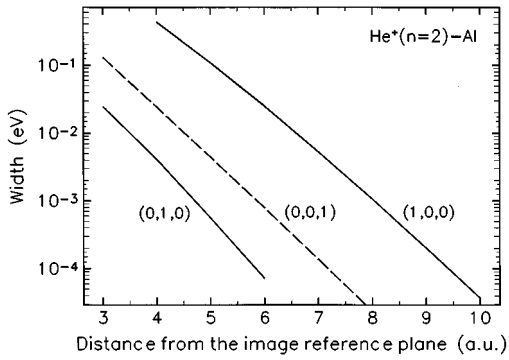

FIG. 2. Widths of the He^+ $(n=2)$ states in front of an Al surface. Solid lines: $m=0$ states; dashed line: $|m|=1$ state. Parabolic notations for the states are also given.

surface distance, where the width is too large or too small. The degeneracy of the states is lifted by the surface potential. As in the case of the hydrogen $n=2$ manifold [28], three states are formed. They correspond to the state $|m|=1$ ($\pm$ states are degenerated) and to the two states with $m=0$. Among the $m=0$ states, the state with the largest width has the largest energy. The energy and the width of the $|m|=1$ state are in between those of the $m=0$ states.

These results can be understood if one expands the perturbing potential felt by the electron close to the ion:

$$V_{e\text{-}s}+\Delta V_{e\text{-}s}=\frac{2Q-1}{4R}+\frac{Q-1}{4R^2}Z+\frac{2(Q-2)Z^2-Q\rho^2}{16R^3}+\frac{Z\{(2Q-8)Z^2-3Q\rho^2\}}{32R^4}, \tag{6}$$

where Q is the ion core charge, R is the ion distance from the surface, and Z,ρ are the electron cylindrical coordinates. The coordinate system is centered around the ion with the Z axis normal to the surface, and pointing toward the metal. Close to the ion and for not too small ion-surface distances, the electron-ion distance is small compared to the ion-surface distance and the expression (6) has been obtained by expanding the potential in powers of Z/R and ρ/R. For this expansion, the electron-surface potential has been approximated by the leading image term.

Since the atomic states have a limited spatial extension, the use of a limited expansion around the ion center can be used to discuss the structure of the manifold splitting. The first term in (6) gives the well-known image charge shift of the electron energy. The second term mixes the states with different l inside a manifold; this term corresponds to a constant electrostatic field and thus to the linear Stark effect. The higher-order terms correspond to the fact that the field is not constant; they contribute to the energy shift and to the mixing of the levels. Let us consider the second term in detail. It vanishes in the case of hydrogen; in that case, the level splitting is produced by the nonhomogeneous part of the electric field [28]. For multicharged ions, the second term is present and at large distances it governs the mixing of the different levels inside a manifold; it corresponds to a field equal to

$$\varepsilon=\frac{(Q-1)}{4R^2}. \tag{7}$$

Below, we will use a parabolic notation (k_1,k_2,m) for the various states [31]. This choice is well suited for large-R distances where the linear Stark effect dominates; at smaller R, although a parabolic notation is not adapted anymore, we will keep it by continuity. The parabolic quantum numbers are linked by a quantization relation:

$$k_1+k_2+|m|+l=n, \tag{8}$$

where n is the principal quantum number.

In the $n=2$ manifold we thus have three states: (1,0,0), (0,1,0), and (0,0,1). The case $k_1>k_2$ corresponds to situations where the electron spends more time in the half space $Z>0$. The (1,0,0) state is thus oriented towards the metal, where the coupling with the metal electronic states is larger and so the (1,0,0) state has a larger width than the (0,1,0) state. The (0,0,1) state is centered around the ion and thus has an intermediate width. A similar discussion can be made for the energy of the levels: due to the potential created by the ion core image, the potential $(V_{e\text{-}s}+\Delta V_{e\text{-}s})$ is higher in the $Z>0$ region than in the $Z<0$ region and thus the energy of the (1,0,0) state is higher than that of the (0,1,0) state, with the (0,0,1) state energy in between. It must be stressed that in the case of the $(n=2)$ manifold of hydrogen, the second term of (6) is missing and the above ordering is reversed; i.e., the state with the largest width has the smallest energy [28].

To make a more precise analysis of the energies of the states we can subtract from the calculated values a first-order perturbative estimate for the energy of the $(0,0,m)$ state. Indeed, the $(0,0,m)$ state coincides with the spherical state $\{n,l=n-1,|m|=n-1\}$, which is the $\{2,1,1\}$ state in the $n=2$ manifold. For the spherical state, the first-order perturbative estimate is

$$\Delta E=\langle n,l,m|V_{e\text{-}s}+\Delta V_{e\text{-}s}|n,l,m\rangle, \tag{9}$$

where $l=m=n-1$.

An analytical prediction for ΔE, based on the expansion (6) can be made. Indeed, the first term in (6) leads to the image shift

$$\Delta E_1=\frac{(2Q-1)}{4R}. \tag{10}$$

The second and fourth terms do not contribute to the energy shift of the spherical state because of symmetry. The third term leads to an energy shift equal to

$$\Delta E_3=\frac{(3Q-4)\langle Z^2\rangle_{n,n-1,n-1}-Q\langle r^2\rangle_{n,n-1,n-1}}{16R^3} \tag{11}$$

with the use of the formulas

$$\langle Z^2\rangle_{n,l,m}=\frac{n^2}{2Q^2}[5n^2+1-3l(l+1)]\times\left\{\frac{1}{3}+\frac{2}{3}\frac{2l(l+1)-3m^2}{(2l+3)(2l-1)}\right\},$$

$$\langle r^2\rangle_{n,l,m}=\frac{n^2}{2Q^2}[5n^2+1-3l(l+1)].$$

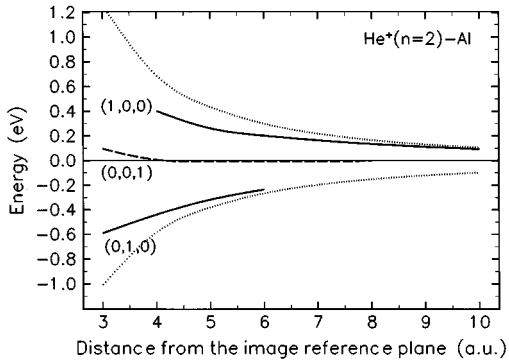

FIG. 3. Stark analysis of the energies of the He^+ $(n=2)$ states in front of an Al surface. The energies are referred to a perturbative estimate for the energy of the (0,0,1) state. Solid lines: $m=0$ states; dashed line: $|m|=1$ state; dotted lines: perturbative estimate for the energies of the $m=0$ states based on the linear Stark effect.

Finally we get

$$\Delta E=\frac{2Q-1}{4R}+\frac{n^2}{32R^3Q^2}[2n^2+3n+1]\times\left\{\frac{(3Q-4)(2n-3)}{4n^2-4n-3}-Q\right\}. \quad (12)$$

We found that at ion-surface distances larger than 15 a.u. formula (12) reproduces the results of the numerical evaluation (9) with an accuracy of the order of a few meV for all the systems studied here.

Figure 3 presents the energies of the states of the $n=2$ manifold referred to the estimate of the energy of the spherical state obtained from (12). One can see that down to rather small ion-surface distances R, the first-order perturbation gives a good estimate for the energy of the (0,0,1) state (dashed line). The energies of the (1,0,0) and (0,1,0) states can also be estimated from the expansion (6). We assume that they can be described as linear Stark states; then first-order perturbation theory gives their energy shift:

$$\Delta E_{(k_1,k_2,m)}=\langle k_1,k_2,m|V_{e\text{-}s}+\Delta E_{e\text{-}s}|k_1,k_2,m\rangle. \quad (13)$$

We only keep the 3 first terms in (6), similarly to the above estimate for the spherical state. In this case,

$$\Delta E_1=\frac{(2Q-1)}{4R}, \quad (14)$$

i.e., the same as (10),

$$\Delta E_2=\frac{3}{2}\frac{n}{Q}(k_1-k_2)\frac{Q-1}{4R^2}, \quad (15)$$

which is the linear Stark splitting

$$\Delta E_3=\frac{(3Q-4)\langle Z^2\rangle_{k_1,k_2,m}-Q\langle r^2\rangle_{k_1,k_2,m}}{16R^3}. \quad (16)$$

ΔE_3 can be calculated by the use of the following formulas:

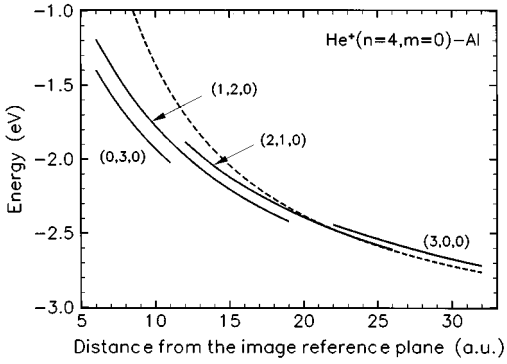

FIG. 4. Energies of the He^+ $(n=4,\ m=0)$ states in front of an Al surface (solid lines). The dotted line represents the energy of the level shifted by the image charge term. Parabolic notations for the states are given.

$$\langle Z^2\rangle_{k_1,k_2,m}=\frac{n^2}{4Q^2}\{n^2+3-m^2+9(k_1-k_2)^2\},$$

$$\langle r^2\rangle_{k_1,k_2,m}=\frac{n^2}{4Q^2}\{7n^2+5-3m^2+3(k_1-k_2)^2\}.$$

Figure 3 presents simple estimates for the energies of the (1,0,0) and (0,1,0) states obtained as the expectation values of the three first terms of (6) for linear Stark states. Although the energies of the states inside the $n=2$ manifold display a Stark-splitting-like pattern [the (1,0,0) and (0,1,0) split almost symmetrically from the spherical state], the simple perturbative estimates are found to quantitatively reproduce the state energies only for large distances. The differences are attributed to the inhomogeneity of the electrostatic field in which the ion is embedded and which results in non-negligible higher-order terms in (6) for the nonspherical states. Indirect coupling between the states with the same symmetry can also occur via the continuum of metallic states [32] and can influence the level widths and energies.

Figures 4, 5, and 6 present the results for the energies of

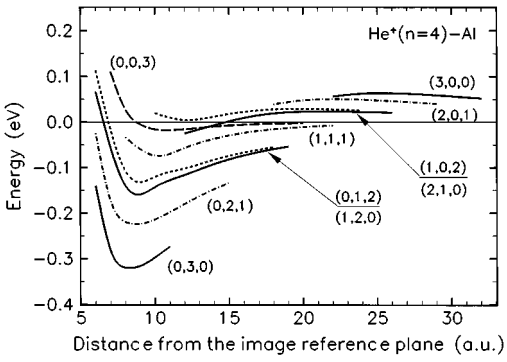

FIG. 5. Energies of the He^+ $(n=4)$ states in front of an Al surface. The energies are referred to a perturbative estimate for the energy of the (0,0,3) state. Solid lines: $m=0$ states; dashed lines: $|m|=1$ states; short-dashed lines: $|m|=2$ states; long-dashed line: $|m|=3$ state. Parabolic notations are given for the states. For the nearly degenerate states, the order of the notations corresponds to the energy order.

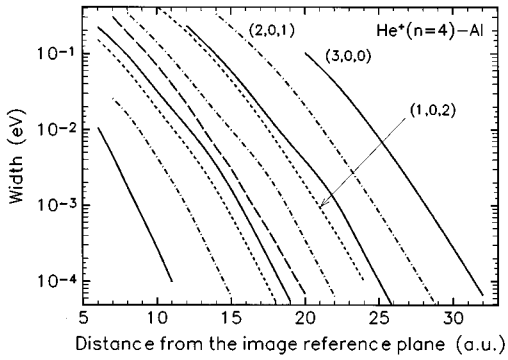

FIG. 6. Widths of the He^+ $(n=4)$ states in front of the Al surface. Solid lines: $m=0$ states; dashed lines: $|m|=1$ states; short-dashed lines: $|m|=2$ states; long-dashed line: $|m|=3$ state. Parabolic notations are given for the states with the largest width within each $|m|$ manifold.

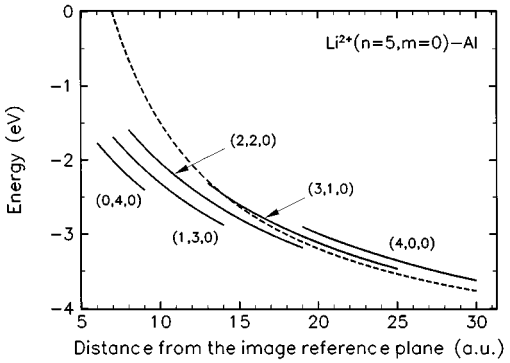

FIG. 7. Energies of the Li^{2+} $(n=5,\ m=0)$ states in front of an Al surface (solid lines). The dashed line represents the energy of the level shifted by the image charge term. Parabolic notations of the states are given.

the states of the $n=4$ manifold of He^+. In this case, 10 hybrid states are formed. These states are (Stark notation)

$$4 \text{ states with } m=0: \quad (3,0,0),(2,1,0),(1,2,0),(0,3,0),$$

$$3 \text{ states with } |m|=1: \quad (2,0,1),(1,1,1),(0,2,1),$$

$$2 \text{ states with } |m|=2: \quad (1,0,2),(0,1,2),$$

$$1 \text{ state with } |m|=3: \quad (0,0,3).$$

Figure 4 presents the energies of the four $(m=0)$ hybrids of the $n=4$ manifold. The energies are found to increase when R decreases, roughly following the image charge prediction at large R. The energies are found to display a pattern characteristic of the linear Stark splitting, i.e., the energies of the states with the successive values of (k_1-k_2) are roughly equidistant. Figure 5 further illustrates this point by showing the energies of the ten states of the manifold relative to the perturbative estimate for the energy of the spherical state (0,0,3). Similarly to the $(n=2)$ case, the perturbative estimate obtained as the expectation value of the first three terms of (6) for the spherical state (0,0,3) is found to reproduce rather well the energy of the spherical state. In the case of the linear Stark effect, the energy of the various hybrids only depends on the difference (k_1-k_2) between the parabolic quantum numbers. In Fig. 5, one can see that the energies of the ten states display a similar pattern: the energies of the states are well ordered according to (k_1-k_2) and the hybrids with the same (k_1-k_2) difference and different m have very similar energies [see, e.g., the (0,1,2) and (1,2,0) states]. This is particularly true at large R; however, for short R distances, deviations from the simple linear Stark picture appear and, for example, the energies of the different hybrids are not equidistant. Estimates for the hybrid state energy based on the linear Stark wave functions and the expansion (6) (not shown in the figure) compare to the CAM results in a way similar to the $(n=2)$ manifold: the agreement is excellent at large R and quickly worsens as R decreases. This again is attributed to inhomogeneities in the field and couplings between the Stark hybrids.

Figure 6 presents the results for the widths of the ten hybrids of the $(n=4)$ manifold of He^+. As the main feature, the widths of the different hybrids differ by orders of magnitude at the same atom-surface distance. Indeed, due to the large number of states in the, e.g., $(m=0)$ subspace, very long-lived and very short-lived hybrids can be formed. Interestingly, in the same way as the hybrid energies mainly depend on the (k_1-k_2) number, the width of the state also mainly depends on (k_1-k_2). As examples, the $(m=2)$ states have widths very similar to those of the $(m=0)$ states with the same (k_1-k_2) and the $(m=1)$ state widths lie in between those of the $(m=0)$ states. In other words, inside each m subspace, the curves for the widths as functions of R appear to be equidistant, the distance between the curves being roughly the same for all the m subspaces. This feature will be further discussed in Sec. IV.

B. Li^{2+}, $n=5$ manifold

In this case, 15 hybrids are expected:

$$m=0: \quad (4,0,0),(3,1,0),(2,2,0),(1,3,0),(0,4,0),$$

$$m=1: \quad (3,0,1),(2,1,1)(1,2,1),(0,3,1),$$

$$m=2: \quad (2,0,2),(1,1,2),(0,2,2),$$

$$m=3: \quad (1,0,3),(0,1,3),$$

$$m=4: \quad (0,0,4).$$

Figure 7 presents the energy of the various $(m=0)$ hybrids as a function of R, together with the simple prediction based on the image charge shift $[(2Q-1)/4R]$. From this simple image shift prediction, one expects the hybrid energy to cross the vacuum level at a distance around $7a_0$ (the distances are measured from the image reference plane), and even to cross at larger distances in the case of the upper Stark hybrids. However, the CAM results are found not to cross the vacuum level. As for the previous systems, the states with the largest energies have the largest widths (see Figs. 7 and 9) and as R decreases, very quickly these states cannot be accurately determined by the CAM method any more. This means that the widths of the states become too large, i.e., that these states cannot be distinguished from the continuum of metal states. As a consequence any population on

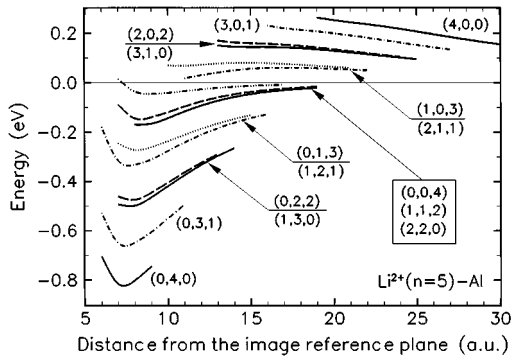

FIG. 8. Energies of the $Li^{2+}(n=5)$ states in front of an Al surface. The energies are referred to a perturbative estimate for the energy of the (0,0,4) state. Solid lines: $m=0$ states; dashed lines: $|m|=1$ states; long-dashed lines: $|m|=2$ states; dotted lines: $|m|=3$ states; dashed triply dotted line: $|m|=4$ state. Parabolic notations are given for the states. For the nearly degenerate states, the order of the notations corresponds to the energy order.

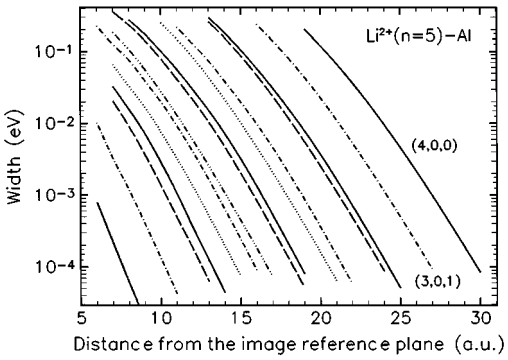

FIG. 9. Widths of the Li^{2+} $(n=5)$ states in front of an Al surface. Solid lines: $m=0$ states; dashed lines: $|m|=1$ states; long-dashed lines: $|m|=2$ states, dotted lines: $|m|=3$ states; dashed triply dotted line: $|m|=4$ state. Parabolic notations are given for the states with the largest width within $m=0$ and $|m|=1$ manifolds.

these states will be quickly ionized. In contrast, the states with the smallest widths can be computed down to small R and are found to have energies smaller than the simple image shift estimate and well below the vacuum level. This result is very similar to that we found in the high-n manifold of He in front of an Al surface [33]. Close to the surface, one finds an energy distribution of the resonances that is quite different from what can be expected from the energy structure of the free atom-ion levels. Only a few states can be found as defined resonances and all of them have energies below vacuum level. No promotion of the states above the vacuum level was observed. To check this idea, we performed a scattering calculation for positive electron energies (above vacuum level). No resonance was found in this range. The above discussion leads to an interesting consequence for the ''peeling off'' phenomenon, often invoked in the discussion of the electron emission in multicharged ion impact on metal surfaces (e.g., [21]). The promotion of the electron energy as R decreases seen in Fig. 7 cannot lead to electron emission, the states decaying by electron emission into the metal. Electron emission into the vacuum will then be only possible at small distances, when the direct interaction between the ion and the metal surface will take place.

Figure 8 presents the energy of the 15 states of the $(n=5)$ manifold. The energies are referred to the energy of the spherical (0,0,4) state obtained by the perturbative estimate discussed above [expectation value of the first three terms of (6)]. This perturbative estimate is rather close to the exact CAM value at large R. The energies of the 15 states display the pattern characteristic of the linear Stark splitting: the energies of the states with the same (k_1-k_2) difference are very close to one another, and the energies of the states differing by one unit of (k_1-k_2) are almost equally spaced. These features are particularly well marked at large R, where a linear Stark splitting is expected; however, even at smaller R, the distribution of energies still closely resembles a linear Stark splitting pattern. The results for the widths of the states are presented in Fig. 9. As for the previous cases, the hybrids have extremely different widths. For example, the difference between two successive states, (4,0,0) and (3,1,0), is around 2 orders of magnitude, whereas the maximum difference between the (4,0,0) and (0,4,0) widths can be estimated around 5 or 6 orders of magnitude. One can also notice the great similarity of the widths of the states having the same (k_1-k_2) difference, i.e., almost the same energy. Except for possibly the larger m values, the widths as functions of R appear as almost equally spaced curves in Fig. 9. This again shows that even if the present situation is not that of the linear Stark effect, the quantity (k_1-k_2) is still a very significant characteristic of the hybrids.

C. O^{7+}, $n=9$ manifold

One expects the formation of 45 hybrids in the $n=9$ manifold of O^{7+}. The results for some of these states will be presented here. In the linear Stark notation these are

$$m=0:\quad (8,0,0),(7,1,0),(6,2,0),(5,3,0),(4,4,0),(3,5,0),$$

$$m=1:\quad (7,0,1),(6,1,1),(5,2,1),(4,3,1),(3,4,1),$$

$$m=6:\quad (2,0,6),(1,1,6),$$

$$m=7:\quad (1,0,7),(0,1,7),$$

$$m=8:\quad (0,0,8).$$

Figure 10 presents the energy of the $(m=0)$ states compared to that of the image charge repulsion prediction $[(2Q-1)/4R]$. Similarly to the previous sections, the energy of the hybrids is found to increase when R decreases, roughly following the image charge prediction at large R; at smaller R, the hybrid energies are well below this estimate.

Figure 11 presents the energy of 16 hybrids, relative to the perturbative estimate for the (0,0,8) spherical state. For the low-m hybrids ($m=0$ and $m=1$), the energy pattern is very close to a linear Stark splitting pattern with energies equally spaced according to the (k_1-k_2) difference. The states with the largest m values $(n=6,7,8)$ are slightly out of this regular pattern, at least for the intermediate range of R where they had been computed.

Figure 12 presents the widths of the same states as Fig. 11. We again observe the same features. The widths are very

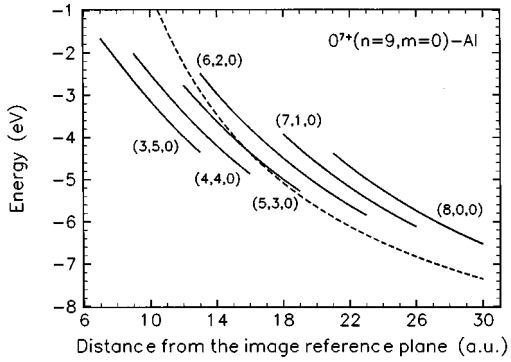

FIG. 10. Energies of the O^{7+} $(n=9, m=0)$ states in front of an Al surface (solid lines). The dashed line represents the energy of the level shifted by the image charge term. Parabolic notations for the states are given.

different and almost scale according to the (k_1-k_2) difference. This is particularly true for the low-m hybrids, the higher-m hybrids being slightly out of this scale.

IV. SCALING FOR THE WIDTHS

It has already been mentioned above that there is a regularity in the hybrid dependence of the width. This is further stressed in Fig. 13, which presents the widths for the $(m=0)$ and $(m=1)$ hybrids in the case of Li^{2+} $(n=5)$ manifold. The various curves for the $m=0$ widths as functions of R appear to be shifted one from the other by a constant ΔR shift, and the $(m=1)$ curves display the same ΔR shift. This feature can be understood in terms of the linear Stark effect. In a Stark hybrid, the electron density is displaced from the ion center and the average displacement is given by (linear Stark effect for a pure Coulomb field)

$$\langle Z\rangle=\frac{3}{2}\frac{n}{Q}(k_1-k_2).$$

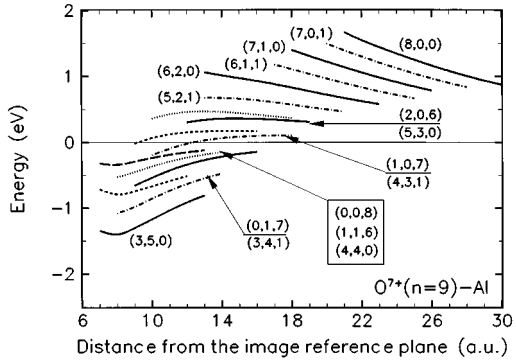

FIG. 11. Energies of some of the O^{7+} $(n=9)$ states in front of an Al surface. The energies are referred to a perturbative estimate for the energy of the (0,0,8) state. Solid lines: $m=0$ states; dashed lines: $|m|=1$ states; dotted lines: $|m|=6$ states; short-dashed lines: $|m|=7$ states; long-dashed line: $|m|=8$ state. Parabolic notations are given for the states. For the nearly degenerate states the order of the notations corresponds to the energy order.

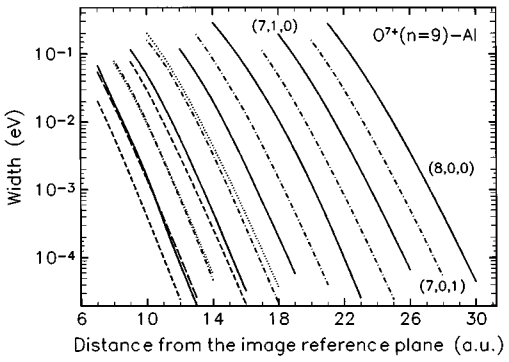

FIG. 12. Widths of some of the $O^{7+}(n=9)$ states in front of an Al surface. Solid lines: $m=0$ states; dashed lines: $|m|=1$ states; dotted lines: $|m|=6$ states; short-dashed lines: $|m|=7$ states; long-dashed line: $|m|=8$ state.

As discussed above, the shift of the electron density is proportional to the difference between the parabolic quantum numbers and can be either positive or negative. This shift is rather large; for the Li^{2+} $(n=5)$ manifold, it amounts to 10 a.u. for the (4,0,0) state and to 5 a.u. for the (3,1,0) state. Since the width is directly related to the overlap between metallic and atomic (Stark hybrids in the present case) electronic wave function, this shift of the electron density can be used to derive a scaling law for the width of the different hybrids. Let us define a scaled atom-surface distance for each (k_1,k_2,m) hybrid:

$$R^{\text{scaled}}(k_1,k_2,m)=R-\frac{3}{2}\frac{n}{Q}(k_1-k_2).$$

Figure 14 presents the results of the widths of various hybrids as functions of the scaled distance. It presents the widths of the $m=0$ and $|m|=1$ hybrids of the $He^{+}(n=4)$, $Li^{2+}(n=5)$, and $O^{7+}(n=9)$ manifolds. All these widths are found to scale rather well inside each system, thus confirming the strong linear Stark effect character of the various hybrids. The scaling is not perfect and in particular, the scaled widths depend on m. This can be seen in Figs. 6, 9, and 12, where the states with the same (k_1-k_2) and different m have similar but not equal widths. However, the scaling works rather well inside each group of states with the same m.

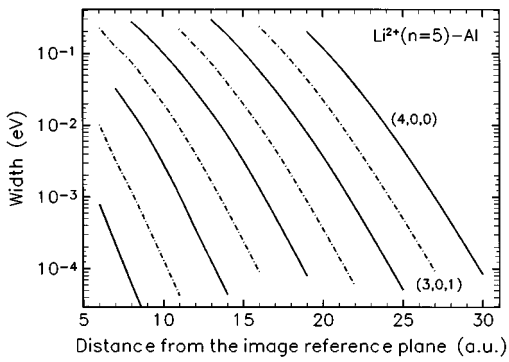

FIG. 13. Widths of the Li^{2+} $(n=5,\ m=0,$ and $|m|=1)$ states in front of an Al surface. Solid lines: $m=0$ states; dashed-dotted lines: $|m|=1$ states. Parabolic notations are given for the states with the largest width within $m=0$ and $|m|=1$ manifolds.

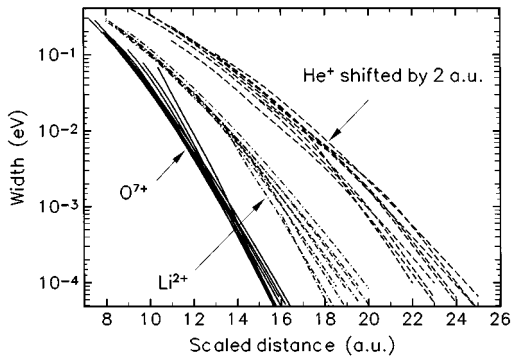

FIG. 14. Dependence of the widths of the $m=0$ and $|m|=1$ states of the He^+ $(n=2)$, Li^{2+} $(n=5)$, and O^{7+} $(n=9)$ manifolds on the scaled distance from the Al surface. Solid lines: O^{7+} $(n=9)$ states; dashed-dotted lines: Li^{2+} $(n=5)$ states; dashed lines: He^+ $(n=2)$ states. The scaled distances of the He^+ $(n=2)$ states are increased by 2 a.u. to separate the He^+ and Li^{2+} results.

V. CONCLUDING SUMMARY

The nonperturbative CAM method has been used to determine the energy and width of one electron multicharged ion state interacting with an Al surface. The He^+ $(n=2,\ n=4)$, Li^{2+} $(n=5)$ and O^{7+} $(n=9)$ manifolds were studied. The interaction with the surface lifts the degeneracy of the hydrogenic levels, resulting in the formation of hybrids. These have very different energies and widths in front of the surface. The hybrid formation can be understood in terms of a linear Stark effect induced by the electron interaction with its electrical image and the ion core image. At large atom-surface distances, the energy of the states can be accurately determined using a simple first-order perturbation approach. At smaller distances, this estimate is not accurate any more, although the pattern of the energies and the widths of the hybrids resemble very much that of a linear Stark splitting. The differences are attributed to the inhomogeneities of the field, to possible indirect couplings between the states via the continuum [32,33], and to possible intermanifold couplings. It must be stressed that the hybrid formation is associated with a rather large displacement of the electronic cloud away from the ion center, which can then sample the electrostatic field in a rather large region and can then easily feel its inhomogeneity.

The present results for the widths are found to be rather different from those predicted by the analytical formulas given in [19,20]. The discrepancy increases when n increases and can reach 2 orders of magnitude for the O^{7+}, $n=8$, (8,0,0) state. Such discrepancies between exact and analytical approaches have already been reported in the case of H atoms in front of an Al surface [26]. A comparison of the present results with the perturbative results of Wille [22–24] will be presented elsewhere [34].

The energy of the hybrids is found to increase when the ion approaches the surface, however, without crossing the vacuum level. At small R, only a few states survive with a moderate width; all the other states, being extremely broad, have disappeared due to the coupling with the metal.

The widths of the hybrids as functions of the distance from the surface are found to present a very regular pattern. A scaling law has been proposed for these widths. It is based on the fact that, in a Stark hybrid, the electronic cloud is shifted from the ion center and the width is then a function more of the distance between the electronic cloud and the surface than of the ion-surface distance.

The fact that the different hybrids have very different widths will indeed influence the electron capture by bare multicharged ions. In a given manifold, the state with the largest k_1, i.e., with the electronic cloud shifted toward the metal, has the largest width and is then preferentially populated if it is below the Fermi level. This feature will lead to a strong polarization of the states populated by resonance electron capture. In the case of successive electron capture, one can expect the same feature to be present and so the hollow atoms that are formed by multiple electron capture will also be highly polarized, with the electronic cloud strongly pointing toward the metal. This will indeed strongly influence the decay of the hollow atom. In addition, since the state with the largest width is also the one with the highest energy, it will be the first one to be ionized when the manifold energy will go above the Fermi energy.

[1] H. J. Andrä, in *Physics of Highly Ionized Atoms*, edited by R. Marrus (Plenum, New York, 1989).
[2] P. A. Zeijlmans van Emmichoven, C. C. Havener, and F. W. Meyer, Phys. Rev. A **43**, 1405 (1991).
[3] F. Aumayr, H. Kurz, D. Schneider, M. A. Briere, J. W. McDonald, C. E. Cunningham, and H. P. Winter, Phys. Rev. Lett. **71**, 1943 (1993).
[4] H. Kurz, F. Aumayr, C. Lemell, K. Töglhofer, and H. P. Winter, Phys. Rev. A **48**, 2182 (1993).
[5] R. Köhrbrück, S. Hustedt, S. Shippers, W. Heiland, J. Bleck-Neuhaus, J. Kemmler, D. Lechter, and N. Stolterfoht, Nucl. Instrum. Methods Phys. Res. Sect. B **78**, 93 (1993).
[6] R. Köhrbrück, M. Grether, A. Spieler, N. Stolterfoht, R. Page, A. Saal, and J. Bleck-Neuhaus, Phys. Rev. A **50**, 1429 (1994).
[7] P. Varga and U. Diebold, in *Low Energy Ion-Surface Interactions*, edited by J. W. Rabalais (John Wiley & Sons, Chichester, 1994), p. 355.
[8] T. Neidhart, F. Pichler, F. Aumayr, H. P. Winter, M. Shmid, and P. Varga, Phys. Rev. Lett. **74**, 5280 (1995).
[9] J. Limburg, S. Shippers, R. Hoekstra, R. Morgenstern, H. Kurz, F. Aumayr, and H. P. Winter, Phys. Rev. Lett. **75**, 217 (1995).
[10] J. Burgdörfer and F. Meyer, Phys. Rev. A **47**, R20 (1993).
[11] H. Winter, C. Auth, R. Schuch, and E. Beebe, Phys. Rev. Lett. **71**, 1939 (1993).
[12] H. Winter, Europhys. Lett. **18**, 207 (1992).
[13] C. Auth, T. Hecht, T. Igel, and H. Winter, Phys. Rev. Lett. **74**, 5244 (1995).
[14] J. Burgdörfer, P. Lerner, and F. W. Meyer, Phys. Rev. A **44**, 5674 (1991).

[15] J. Burgdörfer, in *Review of Fundamental Processes and Applications of Atoms and Ions*, edited by C. D. Lin (World Scientific, Singapore, 1993), p. 582.
[16] R. Brako and D. M. Newns, Rep. Prog. Phys. **52**, 655 (1989).
[17] J. J. C. Geerlings, J. Los, J. P. Gauyacq, and N. M. Temme, Surf. Sci. **172**, 257 (1986).
[18] D. G. Langreth and P. Nordlander, Phys. Rev. B **43**, 2541 (1991).
[19] T. P. Grozdanov and R. Janev, J. Phys. B **10**, 1385 (1977); R. K. Janev, *ibid*. **7**, 1506 (1974); **7**, L359 (1974).
[20] N. N. Nedeljkovic, FIZIKA **12**, 275 (1980).
[21] J. W. Gadzuk, Surf. Sci. **6**, 133 (1967); **6**, 159 (1967).
[22] U. Wille, Nucl. Instrum. Methods Phys. Res. Sect. B **79**, 132 (1993).
[23] U. Wille, Surf. Sci. **307-309**, 874 (1994).
[24] U. Wille, Phys. Rev. B **50**, 1888 (1994).
[25] P. Nordlander and J. C. Tully, Phys. Rev. Lett. **61**, 990 (1988).
[26] P. Nordlander and J. C. Tully, Phys. Rev. B **42**, 5564 (1990).
[27] D. Teillet-Billy and J. P. Gauyacq, Surf. Sci. **239**, 343 (1990).
[28] A. G. Borisov, D. Teillet-Billy, and J. P. Gauyacq, Nucl. Instrum. Methods Phys. Res., Sect. B **78**, 49 (1993).
[29] P. J. Jennings, R. O. Jones, and M. Weinert, Phys. Rev. B **37**, 6113 (1988).
[30] D. Teillet-Billy and J. P. Gauyacq, Surf. Sci. **269/270**, 62 (1992).
[31] L. Landau and E. Lifchitz, *Mecanique Quantique* (Mir, Moscow, 1975).
[32] G. E. Makhmetov, A. G. Borisov, D. Teillet-Billy, and J. P. Gauyacq, Europhys. Lett. **27**, 247 (1994).
[33] G. E. Makhmetov, A. G. Borisov, D. Teillet-Billy, and J. P. Gauyacq, Nucl. Instrum. Methods Phys. Res. Sect. B **100**, 342 (1995).
[34] U. Wille and A. G. Borisov, Surf. Sci. **338**, L875 (1995).